

High-performance natural rubber nanocomposites with marine biomass (tunicate cellulose)

Liming Cao · Xingfeng Fu · Chuanhui Xu · Shiheng Yin · Yukun Chen

Received: 15 January 2017 / Accepted: 17 April 2017 / Published online: 6 May 2017
© Springer Science+Business Media Dordrecht 2017

Abstract Due to the importance in economic and environmental benefits, marine biomass has gained increasing attention in recent years. In this work, marine biomass-based materials were prepared and characterized. Highly reinforcing cellulose nanocrystals (CNCs) with length of 1–2 μm and aspect ratio of ~ 75 were extracted from tunicates (t-CNCs), and CNCs with length of 100–300 nm and aspect ratio of ~ 15 from cotton (c-CNCs) were presented for comparison. In order to enhance interfacial interactions between CNCs and rubber, modification of natural rubber (NR) was conducted via epoxidation reaction to obtain epoxidized NR (ENR). Fully bio-based rubber nanocomposites were produced by latex mixing. Compared with NR

nanocomposites, hydrogen bonding formed between ENR and CNCs, which led to homogeneous dispersion of CNCs and enhanced interfacial adhesion between them. Moreover, t-CNCs with longer length and larger aspect ratio facilitate filler entanglements, which led to higher reinforcing efficiency. Consequently, both hydrogen bonding and filler entanglements contributed to the improved mechanical properties of ENR/t-CNCs nanocomposites.

Keywords Cellulose nanocrystals · Modification · Hydrogen bonding · Filler entanglements · Mechanical reinforcement

L. Cao · X. Fu · Y. Chen (✉)
The Key Laboratory of Polymer Processing Engineering,
Ministry of Education, South China University of
Technology, Guangzhou 510640, China
e-mail: cyk@scut.edu.cn

S. Yin (✉)
Analytical and Testing Center, South China University of
Technology, Guangzhou 510640, China
e-mail: shhyin@scut.edu.cn

C. Xu
School of Chemistry and Chemical Engineering, Guangxi
University, Nanning 530004, China

C. Xu · Y. Chen
The State Key Laboratory of Pulp and Paper Engineering
of China, South China University of Technology,
Guangzhou 510640, China

Introduction

Nowadays, with the development and utilization of marine resources, more attention is focused on extracting industrial materials from marine biomass, such as alginate fibers (Miura et al. 1999; Balakrishnan et al. 2005), chitin (Zeng et al. 2012; Yi et al. 2005), cellulose (Zhao and Li 2014), etc. Among them, cellulose nanocrystals (CNCs), which can be extracted from a marine animal, namely tunicates, are considered to be one of the most promising industrial materials (Zhao et al. 2015; Wagner et al. 2016; Habibi et al. 2010).

CNCs, which are highly crystalline rod-like particles, are currently attracting particular interest in both academia and industry, due to the abundance, excellent renewability, appealing outstanding mechanical

properties and nanoscale dimensions, imparting to them a very high surface area (Moon et al. 2011; Lin et al. 2012; Hu et al. 2013). Favier and co-workers (Favier et al. 1995a; Favier et al. 1995b) performed the earliest study of using CNCs as a reinforcing phase in a matrix of latex nanocomposites, and firstly demonstrated the reinforcing effect of CNCs in polymers. Since then, there has been growing interest in using CNCs as fillers in polymer matrix, involving different kinds of CNCs as well as a broad range of polymeric matrixes (Samir et al. 2004; Tang and Weder. 2010; Khelifa et al. 2012; Cao et al. 2013a, b; Ma et al. 2017; Wu et al. 2016).

However, most attention has been focused on CNCs derived from land resources, such as cotton (Cao et al. 2013a, b), wood (Moon et al. 2011; Lin et al. 2012) and ramie (Khelifa et al. 2012), among others, and concern regarding cellulose resources from marine resources has been limited. Among the marine resources, tunicates are the only known marine animal that produces cellulose. Tunicate cellulose exists naturally in the outer tissues, termed tunic (Zhao and Li 2014; Zhao et al. 2015), which is treated as a byproduct and always thrown away as waste. Therefore, extracting CNCs from tunicates has important economic and environmental benefits. Moreover, compared with CNCs isolated from other resources, tunicate CNCs (t-CNCs) show longer length and a higher aspect ratio (Habibi et al. 2010; Samir et al. 2004), which facilitates CNC entanglements and filler network formation. Therefore, nanocomposites comprising t-CNCs may display more pronounced properties.

NR is a biopolymer, which has been extensively used in the field of automotive tires and other applications (Xu et al. 2016). CNC-filled NR nanocomposites are explored and enhanced mechanical properties are achieved (Riyajan et al. 2009; Nontasorn et al. 2005). In order to fully exhibit the reinforcement potential of fillers in rubber, both strong interfacial interactions and fine dispersion of fillers in the matrix are essential (Chen et al. 2016, 2017; Yue et al. 2013). However, the hydrophobic nature of a NR matrix is incompatible with hydrophilic CNCs, and the weak interfacial interactions are insufficient to produce a satisfactory enhancement. In order to improve the interfacial interactions between NR and CNCs, Mariano et al. (Mariano et al. 2016) explored oxidization of NR latex by using KMnO_4 as an oxidant, and hydrogen bonding formed between the

hydroxyl groups of oxidized NR and CNCs. However, the higher oxidation level led to a decrease of NR's molecular weight, which resulted in the deterioration of the properties of the nanocomposites.

Meanwhile, epoxidation of NR via hydrogen peroxide and formic acid, which is a green and pollution-free method compared with Mariano's work (Mariano et al. 2016), produces randomly distributed epoxy and hydroxyl groups (Yu et al. 2008; Bradbury and Perera 1988), and there has been commercial-grade epoxidized NR (ENR). The introduction of epoxy groups endows ENR new properties, except for the normal characteristics of NR, such as reduced gas permeability, improved oil resistance, etc. In addition, the existence of polar epoxy groups may enhance the reinforcing efficiency and improve dispersion of CNCs via hydrogen bonding.

In the present work, for better utilization of marine resources, CNCs were extracted from tunicates and were explored in regards to their potential use as reinforcing filler for bio-based rubber. Moreover, CNCs with short length were isolated from cotton (c-CNCs) for comparison. Considering the polar nature of CNCs, we employed a simple, green and eco-friendly method to introduce polar epoxy groups onto NR molecules via epoxidation reaction. Fully bio-based rubber nanocomposites were fabricated by mixing aqueous CNC suspension with ENR latex and subsequent co-coagulation. By introducing epoxy groups onto NR molecules, we significantly enhanced the interfacial interactions via hydrogen bonding between hydroxyl groups and epoxy groups. The morphology, mechanical properties and thermal stability of the nanocomposites are investigated using various characterization approaches, and the comparison between t-CNCs and c-CNCs is also carried out.

Experimental

Materials

Natural rubber latex with 60% solids content was supplied by Doubleone Co. Ltd. (Guangzhou, China). Tunicates used in this study were obtained from Weihai, Shandong, China. Cottonseed linter was supplied by Hubei Chemical Fiber Manufacture, China. 99% sodium hydroxide was used for alkaline treatment. Acetic acid and sodium hypochlorite were

used as bleaching agents. 98% formic acid and 30% hydrogen peroxide were used for epoxidation reaction of NR latex. All the reagents were analytical grade and used as received. All the rubber additives, including sulfur (S), zinc oxide (ZnO), steric acid (SA), and *N*-tertbutylbenzothiazole-2-sulphenamide (NS), were industrial grade and used as received.

Preparation of cellulose nanocrystals

t-CNCs were extracted from tunicates, whose mantle is formed of cellulosic microfibrils (tunicin) particularly well-organized and, therefore, highly crystalline. The preparation of t-CNCs was previously described elsewhere (Zhao et al. 2015; Samir et al. 2004). Small fragments of the tunicin were first deproteinized by several successive bleaching treatments. The bleached tunicin (purified cellulose from tunicate) was then disintegrated, and the resulting pulverized tunicin was mixed with 55 wt% H₂SO₄ solution and hydrolysed at 60 °C for 1 h, with continuous stirring. An aqueous suspension of CNCs was obtained. Then, the suspension was subjected to high-speed centrifugation for 10 min, and the precipitate was washed 3 times with deionized water through re-dispersion and re-centrifugation. After sonication, an aqueous suspension of well-individualized CNCs of colloidal dimensions resulted. c-CNC suspension was prepared following the method of our previous work (Cao et al. 2013a, b). Both of the obtained aqueous suspensions revealed obvious Tyndall effects after standing for 1 week at room temperature, which indicates that both are quite stable.

Modification of natural rubber (NR) latex

In order to improve compatibility and interfacial interactions with CNCs, modification of NR latex was conducted. ENR latex with polar epoxy groups was prepared via a simple, green and eco-friendly method according to the works by Yu and co-workers (Yu et al. 2008). Briefly, 33.4 g of NR latex was first diluted with distilled water to a total solid content of 30% and stabilized with nonionic surfactant. After adjustment to pH = 2 with formic acid, 20.2 g of hydrogen peroxide were added into the above NR latex under slow mechanical stirring. The reaction was conducted for 30 h at 30 °C to obtain ENR latex, then the pH value of the latex was adjusted to 7–8 using

NH₃·H₂O, in order to maintain the neutral environment. The molar percentage of epoxy groups was determined by a Fourier transform infrared (FT-IR) method (Yu et al. 2008).

Preparation of ENR/CNC nanocomposites

A desired amount of t-CNC suspension was added into the ENR latex and stirred for 30 min. Then, the mixture was co-coagulated by adding alcohol as the flocculating agent. The co-coagulated compounds were washed with de-ionized water several times until neutral. After that, the compounds were dried at 50 °C overnight until acquiring constant weight. Then, the dried compounds were compounded with rubber ingredients with a two-roll mill and subjected to compression molding at 150 °C for the optimum curing time, which is determined by a UR-203 vulcameter (U-CAN, Taiwan). A series of nanocomposite films with a thickness of around 0.5 mm was prepared and abbreviated as ENR/t-CNCs-*x*, where *x* is the parts per hundred of rubber (phr) of t-CNCs in the nanocomposites. The formulation of the nanocomposites is listed as follows (in phr): ENR 100; ZnO 5; SA 2; NS 1.5; S 1.5. For comparison, NR nanocomposite with 5 phr t-CNCs and ENR nanocomposite with 5 phr c-CNCs were prepared following the same procedure described above and abbreviated as NR/t-CNCs-5 and ENR/c-CNCs-5, respectively.

Characterizations

Field-emission scanning electron microscopy (FE-SEM, Zeiss Merlin, Germany) was used to characterize the morphology of nanocomposites. For SEM imaging, the specimens were frozen in liquid nitrogen, fractured, coated with a thin layer of gold and observed using a Zeiss Merlin SEM. Atomic force microscopy (AFM) was carried out using a Multimode 8 (Bruker, Germany) instrument operated in a tapping mode. A drop of t-CNC suspension was deposited on the freshly cleaved mica substrates and dried overnight under room conditions. In addition, all the measurements were performed at ambient conditions with the instrument mounted in a vibration isolation system. The dimensions of CNCs were estimated from 50 measurements using the associated software.

FT-IR spectroscopy was performed on a Tensor 27 FT-IR spectrometer (Bruker, Germany) at room

temperature. The specimens with thickness of about 0.5 mm were taken at random from sheets and placed flat on the crystal surface. Each spectrum was collected over 32 scans with a resolution of 4 cm^{-1} in the range of $600\text{--}4000\text{ cm}^{-1}$. The background spectra were recorded with Ge crystal contacting air in the absence of specimens.

X-ray photoelectron spectroscopy (XPS) measurements were carried out using an X-ray photoelectron spectrometer (ESCALAB 250Xi, Thermo Scientific, USA) with monochromated Al K_{α} radiation ($h\nu = 1486.6\text{ eV}$). The vacuum degree of the analysis chamber was $10^{-8}\text{--}10^{-7}\text{ Pa}$ and the analysis area was $0.7 \times 0.3\text{ mm}^2$.

X-ray diffraction (XRD) patterns were recorded by a Bruker D8 Advance X-ray diffractometer with a $\text{Cu-K}\alpha$ radiation source and 40-mA current at room temperature. Patterns were recorded by monitoring diffractions from 5° to 40° with a scan speed of $2^{\circ}/\text{min}$. The crystallinity index I_c was determined with the following equation:

$$I_c = 1 - \frac{I_1}{I_2} \quad (1)$$

where I_1 is the intensity of the amorphous phase at about $2\theta = 18^{\circ}$, and I_2 is the intensity associated with the crystalline region of cellulose ($2\theta = 22.5^{\circ}$; Zhao et al. 2015).

Dynamic mechanical analysis (DMA) was performed with a film in tension mode on a DMA 242 C analyser (NETZSCH, Germany). The measurements were carried out on rectangular samples 4 mm in width, 0.5 mm in thickness and 8 mm in length. Measurements were conducted in the temperature range from -60 to $+50\text{ }^{\circ}\text{C}$ at a frequency of 1 Hz with heating rate of $3\text{ }^{\circ}\text{C}/\text{min}$ and oscillating amplitude of $20\text{ }\mu\text{m}$.

Thermogravimetric analysis (TGA) was obtained with a TG 209 F1 (NETZSCH, Germany) apparatus. In a typical experiment, between 5–10mg of specimen was placed in a clean platinum pan after dried at 60°C for 12h and heated from 30°C to 800°C with a rate of $20^{\circ}\text{C}/\text{min}$ under nitrogen atmosphere.

The procedure to measure the cross-link density was as follows: Five weighed test pieces of specimen (m_0) were immersed in toluene at $23\text{ }^{\circ}\text{C}$ in sealed dark vials. Then, the swollen samples were periodically taken out of the toluene and wiped with tissue paper to remove excess solvent, and immediately weighed (w_1)

on an analytical balance. The weight measurements were continued until the samples acquired constant weight. The cross-link density (ν) was calculated from the Flory–Rehner equation (Flory and Rehner 1943),

$$\nu_e = - \frac{\ln(1 - V_r) + V_r + xV_r^2}{V_1 \left(V_r^{\frac{1}{3}} - \frac{V_r}{2} \right)} \quad (2)$$

where

$$V_r = \frac{\frac{m_r}{\rho_r}}{\frac{m_s}{\rho_s} + \frac{m_r}{\rho_r}} \quad (3)$$

V_1 and x are the molar volume and interaction parameters of the solvent ($V_1 = 106.2\text{ cm}^3/\text{mol}$, $x = 0.39$, for toluene), respectively. m_r and ρ_r are the weight and density of rubber (for ENR, $\rho_d = 0.96\text{ g}/\text{cm}^3$), and m_s and ρ_s are the weight and density of solvent (for toluene, $\rho_s = 0.865\text{ g}/\text{cm}^3$), respectively.

Mechanical properties of the nanocomposites were measured with a universal testing machine (UCAN UT-2080, Taiwan) according to ISO 37, with a strain rate of $500\text{ mm}/\text{min}$. The tests were conducted at 50% relative humidity and $23\text{ }^{\circ}\text{C}$. The specimens were conditioned in the measuring environment for 24 h before testing. The results were averaged on five measurements.

Results and discussion

Morphology, crystallinity, and thermal properties of CNCs

CNCs extracted from tunicates and cotton were produced by sulfuric acid hydrolysis. Figure 1a shows the FTIR spectra of the obtained CNCs, which revealed that both t-CNCs and c-CNCs showed typical cellulose structural characteristics. The absorbance peaks around 3341 , 2903 , and 1062 cm^{-1} represent O–H, C–H, and C–O stretching vibrations, respectively (Kargarzadeh et al. 2012; Johar et al. 2012). The peak near 1160 cm^{-1} confirmed the presence of charged sulphate ester bonds on the cellulose chains generated by sulfuric acid hydrolysis (Zhao et al. 2015). The XRD patterns of the isolated CNCs are presented in Fig. 1b. The well-defined crystalline peaks at 14.7° , 16.6° , 22.7° , and 34.5° are observed, corresponding to (110), (110), (002), and (040) lattice

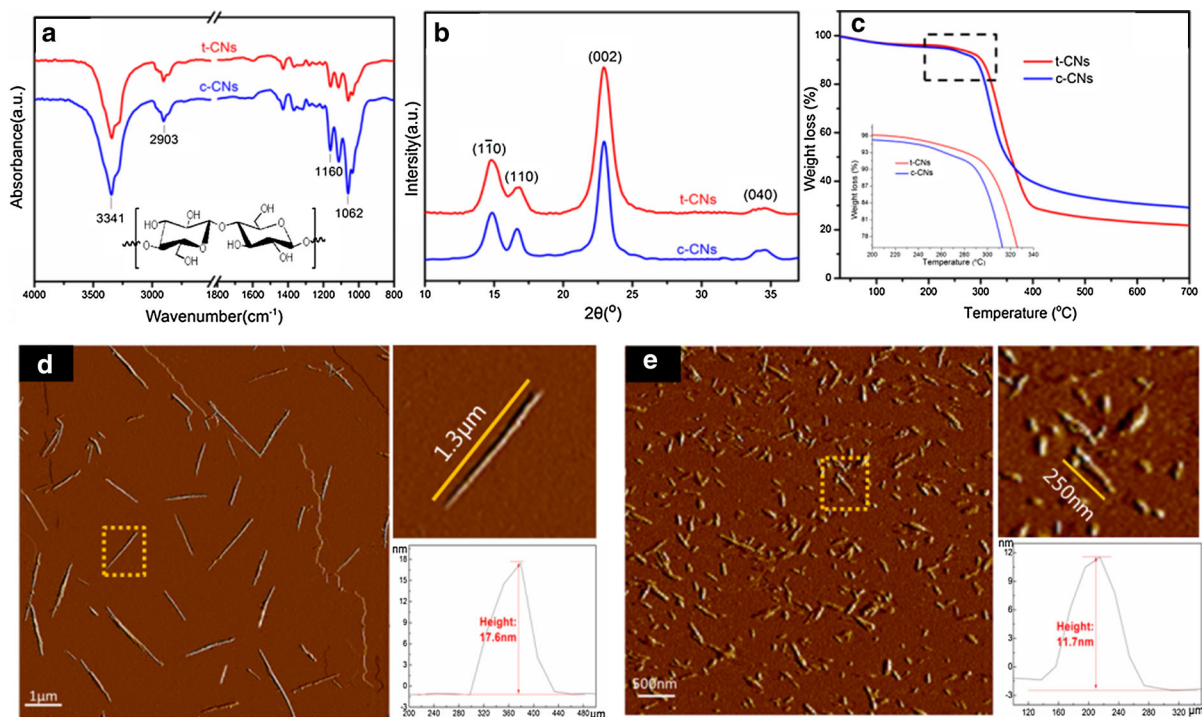


Fig. 1 **a** FT-IR spectra, **b** XRD pattern, **c** thermogravimetric analysis (TGA) graphs of the extracted CNCs, **d** AFM image for t-CNCs, **e** AFM image for c-CNCs

planes, respectively (Bras et al. 2010). The crystallinity index was found to be 88.6% for t-CNCs, which is higher than 80.4% of c-CNCs. Comparatively, t-CNCs showed higher thermal stability than c-CNCs, as illustrated in Fig. 1c. The weight loss between 100 and 200 °C is about 3.6 and 3.8% for t-CNCs and c-CNCs, which represent the water content of the two fillers, respectively. The decomposition of t-CNCs began at approximately 290, 20 °C higher than c-CNCs. The higher crystallinity and larger size, which makes it difficult for heat transfer, may be responsible for the greater thermal stability of t-CNCs. The morphology of t-CNCs and c-CNCs were characterized by AFM as shown in Fig. 1d, e, both CNCs displaying diameters ranging from 10 to 20 nm. While they showed significant difference in length, t-CNCs varied from 500 nm to 2 μm, with a larger aspect ratio of ~75. As a constant, c-CNCs showed length ranging from 150 to 300 nm, with an aspect ratio of ~15. These dimensions agreed well with the reported values from different studies (Habibi et al. 2010; Sacui et al. 2014). The large aspect ratio of t-CNCs is important for their reinforcement.

Interactions between ENR and t-CNCs

It is well-known that the infrared spectrometer is a powerful instrument for the investigation of hydrogen bonding behavior. Figure 2 depicts the FT-IR spectra of NR, ENR and ENR/t-CNC nanocomposites with various t-CNC loadings. As compared with NR in Fig. 2a, the absorption peak around 1664 cm^{-1} of ENR, which is corresponding to the double bond, was weakened. Meanwhile, ENR shows new characteristic absorption peaks around 870 and 1250 cm^{-1} , which were assigned to the asymmetric and symmetric stretching vibrations of epoxy groups generated from the acid-catalyzed epoxidation reaction (Yu et al. 2008; Poh and Lee. 1994). The epoxidation degree was ~40% for the resulting ENR, as calculated from the FT-IR results. Interestingly, with the increase of t-CNCs content, the absorption peak corresponding to the O–H stretching of t-CNCs around 3400 cm^{-1} consistently red-shifted as shown in Fig. 2b, which suggests that hydrogen bonding formed due to the strong interactions between epoxy groups of ENR and hydroxyl groups of t-CNCs.

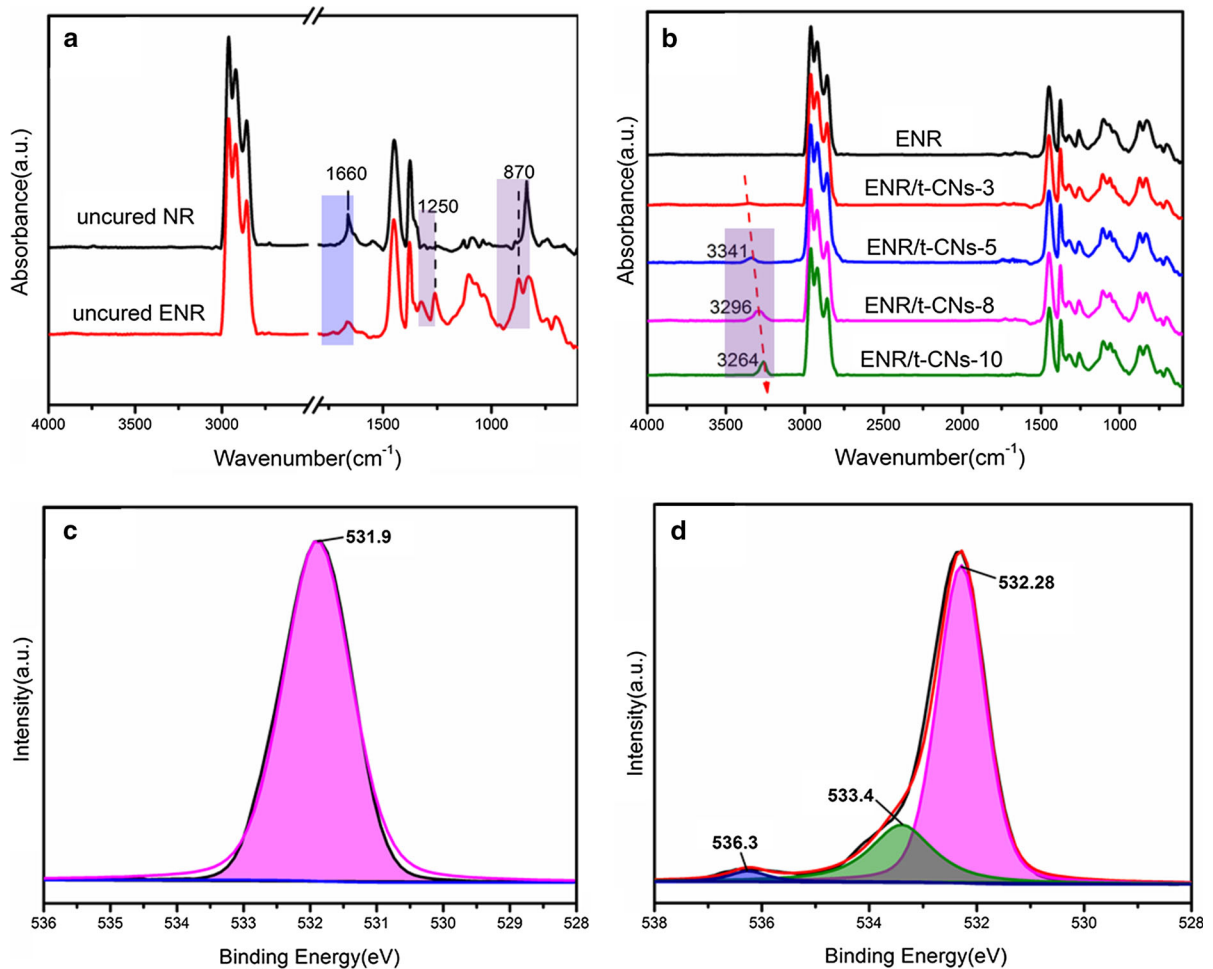


Fig. 2 FT-IR spectra of **a** uncured NR, ENR; **b** cured ENR and ENR/t-CNC nanocomposites; and high-resolution XPS spectra of O 1s for **c** neat ENR; **d** ENR/t-CNCs-10

To further shed light on the interactions between t-CNCs and ENR, XPS measurements were performed. As presented in Fig. 2c, high-resolution XPS spectra of O_{1s} of dried ENR latex shows a chemical environment with binding energy at 531.9 eV, which is assigned to O_{1s} of the C–O–C in ENR. However, Fig. 2d shows that ENR/t-CNCs-10 compound exhibits three species corresponding to bonding energies at 532.3, 533.4 and 536.3 eV, respectively. The latter two species are corresponding to O_{1s} of the C–OH and glucose rings in t-CNCs, respectively. What calls for special attention is that the peak assigned to O_{1s} of C–O–C in ENR shifted from 531.9 to 532.3 eV, indicating that the electron density of the oxygen decreased. This can be regarded as a

result of hydrogen bonding formation between t-CNCs and ENR, because the oxygen of C–O–C in ENR would be partially shared with the hydrogen of the –OH group on t-CNCs in the hydrogen bonding structure (Li et al. 1998).

From the above structure analysis, it can be concluded that strong interface interactions are achieved via hydrogen bonding between t-CNCs and ENR matrix, as illustrated in Fig. 3. The strong interactions between rubber-filler facilitate the even dispersion of t-CNCs within rubber matrix and improve interface adhesion. Moreover, the large aspect ratio of t-CNCs facilitates filler entanglements, which facilitates stress transfer under the deforming process. Both hydrogen bonding and filler

Fig. 3 Illustration of the structure of the ENR/t-CNC nanocomposites

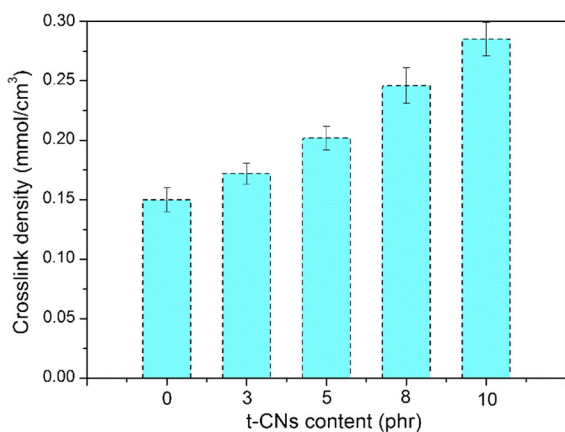
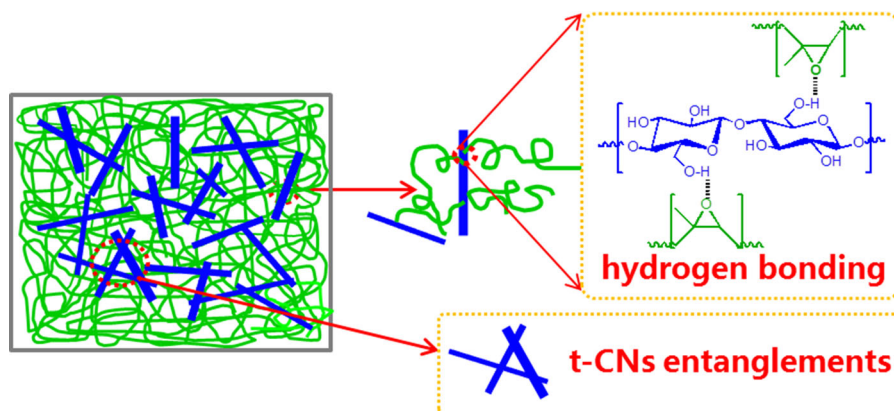


Fig. 4 Cross-link density of neat ENR and ENR/t-CNC nanocomposites

entanglements will have pronounced influence in improving properties of the ENR/t-CNC nanocomposites, as will be discussed below.

Cross-link density analysis

Figure 4 presents the cross-link density determined by solvent swelling measurements by using the Flory–Rehner equation as a function of t-CNC loadings. The ENR/t-CNC nanocomposites showed an increase in cross-link density as compared to neat ENR, and it further increased slightly with t-CNC loading. With only 10 phr t-CNCs, the crosslink density increased to 0.28 mmol/cm⁻³, which is nearly twice as high as in the neat ENR. Strong interfacial interactions via hydrogen bonding between t-CNCs and ENR matrix result in the formation of filler-bound matrix around fillers, which would increase the volume fraction of the rigid phase effectively (Tang and Weder 2010),

Table 1 Curing characteristics of the prepared nanocomposites

Samples	T _{c10} (s)	T _{c90} (s)	M _L (dN.m)	M _H (dN.m)
ENR	135	436	0.52	8.05
ENR/t-CNCs-3	130	467	0.53	8.79
ENR/t-CNCs-5	132	494	0.51	10.14
ENR/t-CNCs-8	129	536	0.54	11.75
ENR/t-CNCs-10	133	572	0.57	13.67

making it more difficult for the solvent to permeate into the matrix, thus reducing the solvent uptake and swelling of the nanocomposites by keeping polymer chains bound together efficiently.

Curing characteristic analysis

The curing characteristics of the prepared nanocomposites cured at 150 °C are summarized in Table 1. It is clear that the incorporation of t-CNCs leads to an obvious increase in maximum torque (M_H). As mentioned above, hydrogen bonding formed between rubber and filler, which restricted motion of rubber chains. The optimum cure time (t_{c90}) also increased with t-CNC content. This can be explained by some of the curing agents being adsorbed onto the t-CNCs' surfaces. Meanwhile, the minimum torque (M_L) showed little difference, which indicates that the addition of t-CNCs has little influence on the processability of the compound. Moreover, as is known, t_{c10} represents the pre-vulcanization characteristic during the process; too low a t_{c10} value will lead to a fast increase of the viscosity of the rubber compound, which makes it difficult to form the designed shape of the products. The t_{c10} values of the compound are

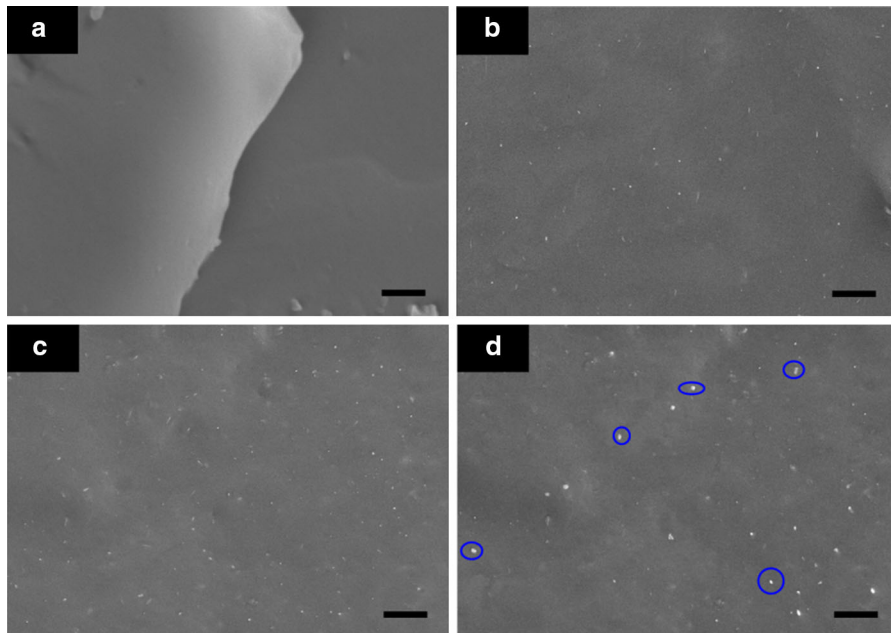


Fig. 5 SEM images of the ENR/t-CNC nanocomposites with different CNC loadings: **a** neat ENR; **b** ENR/t-CNCs-5; **c** ENR/t-CNCs-10; and **d** NR/t-CNCs-5. (scale bar: 2 μm)

almost unchanged with t-CNC content, implying that t-CNCs do not negatively influence the pre-vulcanization process of the ENR matrix.

Scanning electron microscopy

An investigation of the fractured surfaces of ENR and nanocomposites was carried out using SEM to evaluate the dispersion of t-CNCs. Figure 5 shows the SEM images of ENR matrix and the obtained nanocomposites. As compared with neat ENR, the morphology of t-CNCs appeared as white dots, whose relative content detectable on the fracture surface of the nanocomposites increased directly with the filler loading. Those white dots were attributed to the CNCs in the perpendicular plane of the nanocomposites (Barrera and Cornish 2016). Compared with Fig. 5b, d, the dispersion of t-CNCs in NR matrix is uneven, and some aggregates can be observed. While for ENR nanocomposites, no large aggregates and a homogeneous dispersion of t-CNCs were observed, which attests to the good affinity between t-CNCs and ENR matrix. The good affinity should be attributed to the strong interactions via hydrogen bonding between fillers and the matrix. Such uniform dispersion is

anticipated to play an important role in improving properties of the resulted nanocomposites.

Dynamic mechanical thermal analysis

Figure 6 shows the typical tensile storage modulus E' and loss factor $\tan\delta$ as a function of temperature for neat ENR, ENR/t-CNCs-5 and ENR/t-CNCs-10 nanocomposites. As can be easily observed, the DMA traces of all the specimens display a similar behavior, which is glassy below its T_g and exhibits a classical major drop in its E' around the temperature corresponding to the glass–rubber transition, and remains constant with increasing temperature thereafter. As illustrated in Fig. 6a, significant enhancement of E' in both the glassy and rubbery regions upon the incorporation of t-CNCs is observed. For instance, E' of the nanocomposites at $-50\text{ }^\circ\text{C}$ (below T_g) increased from 1.5 GPa for the neat ENR to 2.7 GPa for ENR/t-CNCs-10. While at $25\text{ }^\circ\text{C}$ (above T_g), E' of the nanocomposites represents a 6-fold enhancement over that of neat matrix. The improvement of E' in the glassy region is resulted from the formation of a filler network. While above T_g , the effective volume fraction of the rigid phase is increased because of

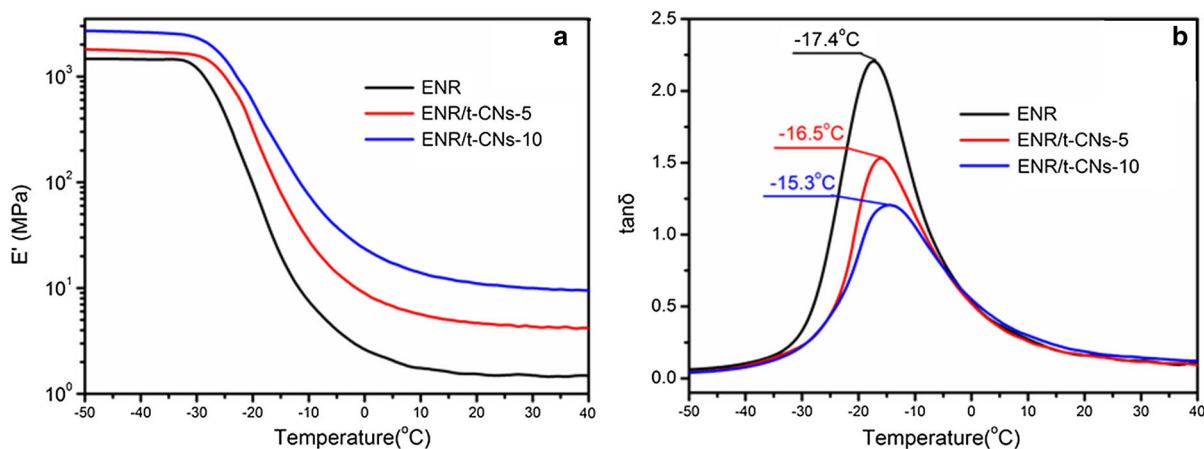


Fig. 6 Typical **a** storage modulus (E') and **b** loss factor ($\tan\delta$) versus temperature curves of neat ENR and its nanocomposites

strong interactions between the filler and matrix, which results in the formation of bounded matrix around fillers and an improved modulus.

Figure 6b displays loss factor $\tan\delta$ as a function of temperature and t-CNC content. $\tan\delta$ of neat ENR shows a maximum value at -17.4 °C, which correlates with the glass–rubber transition of the matrix. The incorporation of t-CNCs slightly shifts the glass transition toward a higher temperature. Most studies have reported that the incorporation of CNCs into polymer matrices seemed not to affect the glass–rubber transition temperature, regardless of the origin of CNCs, the nature of the matrix, or the processing conditions (Habibi et al. 2010). However, in the present study, the segmental movement was restricted due to the strong hydrogen bonding between filler and matrix, which led to T_g shifting toward a higher temperature. Moreover, the increased cross-link density (Fig. 4) was also responsible for the increased T_g . Meanwhile, the amplitude of the damping peak corresponding to the glass transition of ENR decreased with increasing t-CNC loadings, which could be attributed to the greatly restricted motion of ENR chains resulting from the formation of hydrogen bonding between ENR molecules and t-CNCs as indicated by FT-IR and XPS analyses.

Mechanical properties of the nanocomposites

To investigate the effect of t-CNCs as a reinforcing phase in the ENR matrix, the classical tensile tests were performed at room temperature. The typical stress–strain curves of ENR-based nanocomposites

and neat ENR are shown in Fig. 7a, and the tensile properties of the nanocomposites are summarized in Table 2. Clearly, either ENR or nanocomposites with lower t-CNCs content all show nonlinear stress–strain curves, typical behavior of NR, in which strain-induced crystallization behavior occurred at large strain. The strain at which crystallization occurred decreased with the increase of t-CNC content. The filler entanglements and strong interfacial interactions restrict the motion of matrix molecular chains, which oriented at lower strain. The addition of t-CNCs in ENR matrix led to an apparent improvement in the tensile strength, modulus, and stress at 300% as compared to neat ENR. At a t-CNC loading of 5 phr, 3-fold improvement in the stress at 300% strain was obtained, and it further increased by almost 7 times at 10 phr t-CNC loading. The modulus also showed an apparent improvement with increase of t-CNC loadings. While as observed in previous studies (Cao et al. 2013a, b; Bras et al. 2010), strain-to-failure was found to decrease with increase in t-CNC loadings. This is due to the strong interfacial interactions between ENR and t-CNCs via hydrogen bonding, which hold rubber chains more tightly and thus resists the deformation of rubber chains. Work-of-fracture (toughness, proportional to area under the stress–strain curve) increased consistently because of the arresting improved stress and modulus with increasing t-CNC loading. In particular, ENR/t-CNCs-10 showed almost two times higher than neat ENR in work-of-fracture.

However, compared with nanocomposites with lower t-CNC loading (< 5 phr), the specimen with higher t-CNC loading exhibits different stress–strain

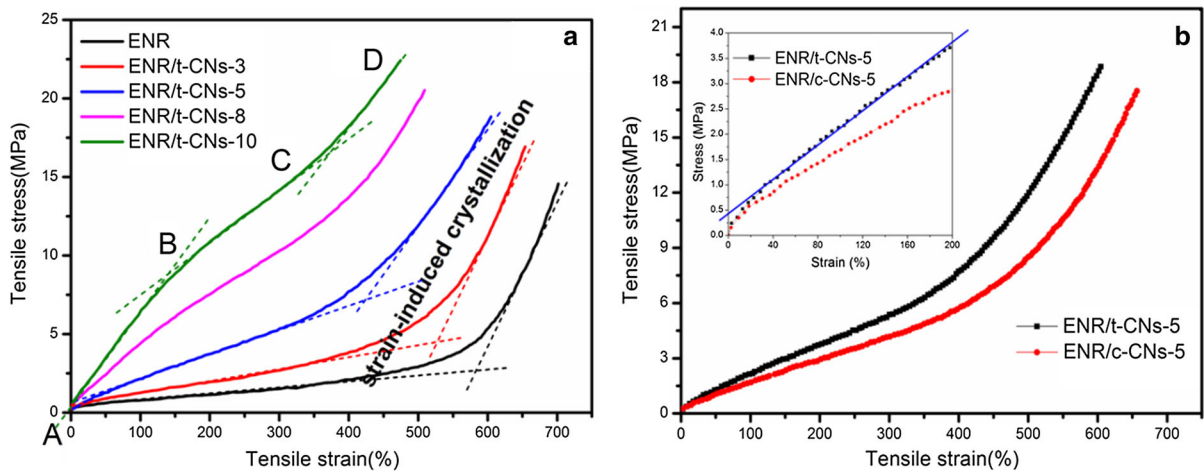


Fig. 7 Tensile stress–strain curves of **a** neat ENR and ENR/t-CNC nanocomposites; **b** comparison between ENR/t-CNCs-5 and ENR/c-CNCs-5

Table 2 Tensile properties of ENR and ENR/t-CNC nanocomposites

Samples	Tensile strength (MPa)	Stress at 300% strain	Strain-to-failure (%)	Modulus (MPa)	Work-of-fracture (MJ/m ³)
ENR	14.4 ± 1.2	1.8 ± 0.5	674 ± 30	4.2 ± 0.6	20.4 ± 3.7
ENR/t-CNCs-3	16.8 ± 1.0	3.5 ± 0.7	608 ± 51	5.1 ± 0.5	28.6 ± 4.4
ENR/t-CNCs-5	18.4 ± 1.3	5.6 ± 0.8	594 ± 38	7.6 ± 0.6	42.7 ± 4.6
ENR/c-CNCs-5	17.6 ± 1.2	4.3 ± 0.6	657 ± 40	6.7 ± 0.5	37.3 ± 4.7
ENR/t-CNCs-8	20.7 ± 2.0	10.2 ± 0.7	510 ± 60	8.8 ± 0.8	47.6 ± 6.3
ENR/t-CNCs-10	22.6 ± 1.6	14.1 ± 1.2	474 ± 60	10.7 ± 1.1	55.9 ± 5.8

behavior, especially for ENR/t-CNCs-10 as shown in Fig. 7a. Three distinguishable deformation regions are observed. Segment [AB]: the quasi-linear elastic deformation region with higher modulus, which is mainly governed by stronger hydrogen bonding and filler network formed at higher filler loading. Segment [BC]: the low-modulus region associated with the destruction of filler network at large deformation, which led to the decrease of the modulus. Hydrogen bonding was still at work at this stage. Segment [CD]: the improved modulus corresponding to the strain-induced crystallization of ENR and hydrogen bonding as well. Namely, the filler network formation and strong hydrogen bonding between filler and matrix contributed to the observed tensile behavior.

In an attempt to compare the reinforcing efficiency of t-CNCs and c-CNCs, Fig. 7b compared the stress–strain curves of ENR/CNC nanocomposites with 5phr t-CNCs and c-CNCs, respectively. Higher reinforcement efficiency of t-CNCs compared to c-CNCs can

be observed, especially for the modulus. Stress increased almost linearly with strain as shown in the insert picture in Fig. 7b, which is mainly attributed to that higher aspect ratio and modulus of t-CNCs leading to more tightly filled entanglements (Tang and Weder 2010). It is also worth noting that the strain at which crystallization (ϵ_c) starts is at around 484% for the ENR/c-CNCs-5 sample, whereas ENR/t-CNCs-5 sample showed a much lower ϵ_c at around 423%. The large aspect ratio of t-CNCs and their entanglements assists in filler–matrix and filler–filler stress transfer (Ten et al. 2012), which facilitates the early occurrence of strain-induced crystallization of the sample.

Conclusions

Highly reinforced t-CNCs with diameter of 10–20 nm, length of 1–2 μm and aspect ratio of ~ 75 were

extracted from tunicates. In order to improve interfacial adhesion, bio-based ENR with an epoxidation degree of ~40% was fabricated via a simple, green and eco-friendly method from NR latex. Hydrogen bonding formed between ENR and CNCs, which facilitated homogeneous dispersion of CNCs as compared with NR. Cross-link density and glass transition temperature improved due to the formation of hydrogen bonding. Moreover, t-CNCs with longer length and large aspect ratio facilitated filler entanglements, and resulted in the improved modulus as compared with ENR/c-CNC nanocomposites. Both hydrogen bonding and filler entanglements contributed to the improved mechanical properties of ENR/t-CN nanocomposites. Inclusion of 10 phr t-CNCs into ENR matrix generated a 7-fold increase in stress at 300% strain, 1.7-fold increase in work-of-fracture, and 57% increase in tensile strength. As a consequence, high-performance, bio-based rubber nanocomposites were prepared by implementing t-CNCs with longer length and larger aspect ratio, together with modification of NR latex through a simple, green, and eco-friendly method.

Acknowledgments This work was financially supported by the State Key Laboratory of Pulp and Paper Engineering of China (Grant No. 201464 and No.201205).

References

- Balakrishnan B, Mohanty M, Umashankar PR, Jayakrishnan A (2005) Evaluation of an in situ forming hydrogel wound dressing based on oxidized alginate and gelatin. *Biomaterials* 26:6335–6342
- Barrera CS, Cornish K (2016) High performance waste-derived filler/carbon black reinforced guayule natural rubber composites. *Ind Crop Prod* 86:132–142
- Bradbury JH, Perera MC (1988) Advances in the epoxidation of unsaturated polymers. *Ind Eng Chem Res* 27:2196–2203
- Bras J, Hassan ML, Bruzesse C et al (2010) Mechanical, barrier, and biodegradability properties of bagasse cellulose whiskers reinforced natural rubber nanocomposites. *Ind Crop Prod* 32:627–633
- Cao XD, Xu CH, Wang YP et al (2013a) New nanocomposites materials reinforced with cellulose nanocrystals in nitrile rubber. *Polym Test* 32:819–826
- Cao XD, Xu CH, Liu YH et al (2013b) Preparation and properties of carboxylated styrene-butadiene rubber/cellulose nanocrystals composites. *Carbohydr Polym* 92:69–76
- Chen YK, Wang YH, Xu CH et al (2016) A new approach to fabricate novel fluorosilicone thermoplastic vulcanizate with bi-crosslinked silicone rubber-core/fluororubber-shell particles dispersed in poly (vinylidene fluoride): Structure and property. *Ind Eng Chem Res* 55(6):1701–1709
- Chen YK, Huang XH, Gong Z et al (2017) Fabrication of high performance magnetic rubber from NBR and Fe₃O₄ via in-situ compatibilization with zinc dimethacrylate. *Ind Eng Chem Res* 56:183–190
- Favier V, Canova GR, Cavaille JY et al (1995a) Nanocomposite materials from latex and cellulose whiskers. *Polym Adv Technol* 6:351–355
- Favier V, Chanzy H, Cavaille JY (1995b) Polymer nanocomposites reinforced by cellulose whiskers. *Macromolecules* 28:6365–6367
- Flory PJ, Jr Rehner (1943) Statistical mechanics of cross-linked polymer networks II. Swelling. *J Chem Phys* 11:512–520
- Habibi Y, Lucia LA, Rojas OJ (2010) Cellulose nanocrystals: chemistry, self-assembly, and applications. *Chem Rev* 110:3479–3500
- Hu X, Xu CL, Gao J et al (2013) Toward environmental-friendly composites of poly(propylene carbonate) reinforced with cellulose nanocrystals. *Compos Sci Technol* 78:63–68
- Johar N, Ahmad I, Dufresne A (2012) Extraction, preparation and characterization of cellulose fibres and nanocrystals from rice husk. *Ind Crop Prod* 37:93–99
- Kargarzadeh H, Abdullah I, Dufresne A et al (2012) Effects of hydrolysis conditions on the morphology, crystallinity, and thermal stability of cellulose nanocrystals extracted from kenaf bast fibers. *Cellulose* 19:855–866
- Khelifa F, Habibi Y, Benard F, Dubois P (2012) Effect of cellulosic nanowhiskers on the performances of epoxidized acrylic copolymers. *J Mater Chem* 22:20520–20528
- Li L, Chan CM, Weng LT (1998) The effects of specific interactions on the surface structure and composition of miscible blends of poly(vinyl alcohol) and poly(N-vinyl-2-pyrrolidone). *Polymer* 39:2355–2360
- Lin N, Huang J, Dufresne A (2012) Preparation, properties and applications of polysaccharide nanocrystals in advanced functional nanomaterials: a review. *Nanoscale* 4:3274–3294
- Ma PM, Shen TF, Lin L et al (2017) Cellulose-g-poly(D-lactide) nanohybrids induced significant low melt viscosity and fast crystallization of fully bio-based nanocomposites. *Carbohydr Polym* 155:498–506
- Mariano M, Kissi NE, Dufresne A (2016) Cellulose nanocrystal reinforced oxidized natural rubber nanocomposites. *Carbohydr Polym* 137:174–183
- Miura K, Kimura N, Suzuki H et al (1999) Thermal and viscoelastic properties of alginate/poly (vinyl alcohol) blends cross-linked with calcium tetraborate. *Carbohydr Polym* 39:139–144
- Moon RJ, Martini A, Nairn J et al (2011) Cellulose nanomaterials review: structure, properties and nanocomposites. *Chem Soc Rev* 40:3941–3994
- Nontasorn P, Chavadej S, Rangsunvigit P et al (2005) Admicellar polymerization modified silica via a continuous stirred-tank reactor system: comparative properties of rubber compounding. *Chem Eng J* 108:213–218
- Poh BT, Lee KS (1994) FTIR study of thermal oxidation of ENR. *Eur Polym J* 30:17–23
- Riyajan SA, Chaiponban S, Tanbumrung K (2009) Investigation of the preparation and physical properties of a novel semi-interpenetrating polymer network based on epoxised NR

- and PVA using maleic acid as crosslinking agent. *Chem Eng J* 153:199–205
- Sacui A, Nieuwendaal RC, Burnett DJ et al (2014) Comparison of the properties of cellulose nanocrystals and cellulose nanofibrils isolated from bacteria, tunicate, and wood processed using acid, enzymatic, mechanical, and oxidative methods. *ACS Appl Mater Interfaces* 6:6127–6138
- Samir MA, Alloin F, Sanchez JY et al (2004) Cellulose nanocrystals reinforced poly(oxyethylene). *Polymer* 45:4149–4157
- Tang LM, Weder C (2010) Cellulose whisker/epoxy resin nanocomposites. *ACS Appl Mater Interfaces* 2:1073–1080
- Ten E, Jiang L, Wolcott MP (2012) Crystallization kinetics of poly(3-hydroxybutyrate-co-3-hydroxyvalerate)/cellulose nanowhiskers composites. *Carbohydr Polym* 90:541–550
- Wagner R, Moon RJ, Raman A (2016) Mechanical properties of cellulose nanocrystals studied by contact resonance atomic force microscopy. *Cellulose* 23:1031–1041
- Wu XD, Han YY, Zhang XX et al (2016) Highly sensitive, stretchable, and wash-durable strain sensor based on ultrathin conductive layer@polyurethane yarn for tiny motion monitoring. *ACS Appl Mater Interfaces* 8:9936–9945
- Xu CH, Cao LM, Lin BF et al (2016) Design of self-healing supramolecular rubbers by introducing ionic crosslinks into natural rubber via a controlled vulcanization. *ACS Appl Mater Interfaces* 8:17728–17737
- Yi H, Wu LQ, Bentley WE et al (2005) Biofabrication with chitosan. *Biomacromol* 6:2881–2894
- Yu HP, Zeng ZQ, Lu G et al (2008) Processing characteristics and thermal stabilities of gel and sol of epoxidized natural rubber. *Eur Polym J* 44:453–464
- Yue YL, Zhang H, Zhang Z et al (2013) Polymer-filler interaction of fumed silica filled polydimethylsiloxane investigated by bound rubber. *Compos Sci Technol* 86:1–8
- Zeng JB, He YS, Li SL et al (2012) Chitin whiskers: an overview. *Biomacromol* 13:1–11
- Zhao YD, Li JB (2014) Excellent chemical and material cellulose from tunicates: diversity in cellulose production yield and chemical and morphological structures from different tunicate species. *Cellulose* 21:3427–3441
- Zhao YD, Zhang YJ, Lindstrom ME et al (2015) Tunicate cellulose nanocrystals: preparation, neat films and nanocomposite films with glucomannans. *Carbohydr Polym* 117:286–296